

Primljen / Received: 25.10.2022.

Ispravljen / Corrected: 16.2.2023.

Prihvaćen / Accepted: 1.3.2023.

Dostupno online / Available online: 10.7.2023.

Scalar and vector-valued fragility analysis of typical Algerian RC bridge piers

Authors:



Assoc.Prof. **Foad Kehila**, PhD. CE
National Earthquake Engineering Research
Center CGS, Algiers, Algeria
Department of Civil Engineering
fkehila@cgs-dz.org
Corresponding author



Assist.Prof. **Mebarek Khelfi**, PhD. CE
National Earthquake Engineering Research
Center CGS, Algiers, Algeria
Department of Civil Engineering
mkhelfi@cgs-dz.org



Assoc.Prof. **Mounir Ait Belkacem**, PhD. CE
National Earthquake Engineering Research
Center CGS, Algiers, Algeria
Department of Civil Engineering
ait_belkacem1@yahoo.fr

Research Paper

Foad Kehila, Mebarek Khelfi, Mounir Ait Belkacem

Scalar and vector-valued fragility analysis of typical Algerian RC bridge piers

This paper presents and discusses an approach for performing scalar and vector vulnerability assessments of typical Algerian RC bridge piers. Across incremental dynamic analysis, the seismic response was calculated while considering 60 seismic ground motions and 10 intensity measures (IMs). An optimal scalar-valued IM was assessed and selected through regression analyses. It was validated based on several metrics including the correlation, efficiency, practicality, and proficiency. The fragility of vector-valued functions that use two pairs of IMs were calculated and compared with fragility curves based on scalars. The comparison indicated that the damage probability can be underestimated or overestimated in vulnerability analysis.

Key words:

fragility curves, incremental dynamic analysis, intensity measure, limit states, seismic performance

Prethodno priopćenje

Foad Kehila, Mebarek Khelfi, Mounir Ait Belkacem

Skalarna i vektorska analiza ranjivosti tipskih AB stupova mostova u Alžiru

Ovaj rad predstavlja i analizira pristup za izvođenje skalarne i vektorske ocjene ranjivosti tipskih AB stupova mostova u Alžiru. Putem inkrementalne dinamičke analize, seizmički je odziv izračunan uzimajući u obzir 60 seizmičkih gibanja tla i 10 mjera intenziteta (IM). Optimalni IM za skalarnu analizu procijenjen je i odabran pomoću regresijske analize. Provjeren je na temelju nekoliko metrika uključujući korelaciju, učinkovitost, praktičnost i sposobnost. Vektorska analiza ranjivosti, uz primjenu dva para IM-ova izračunana je i uspoređena s krivuljama ranjivosti dobivenim skalarnom analizom. Usporedba je pokazala da se u analizi ranjivosti vjerojatnost štete može podcijeniti ili precijeniti.

Ključne riječi:

krivulje ranjivosti, inkrementalna dinamička analiza, mjera intenziteta, granična stanja, seizmičko ponašanje

1. Introduction

Bridges, as essential components of road networks in urban areas and on major highways, are likely to significantly impact traffic and emergency response to earthquake damage.

Such bridges in major earthquake areas need to improve their seismic performance. The objective is to prevent structural collapse of the bridge and effectively manage the remaining states of damage to ensure that the global performance indicators of the bridge are satisfied over the life cycle under potential seismic events at a minimum cost. Therefore, investigations of the seismic performance of bridges subjected to seismic excitation are significant.

RC bridge piers constitute one of the most important components of bridge systems that determine the overall behaviour of bridges during seismic events. Numerous studies aimed at improving the design and seismic performance of bridge piers have been conducted in recent years. Zhou et al. [1] performed a horizontal impact test on reinforced concrete bridge piers with different reinforcement ratios of longitudinal steel bars. Milić et al. [2] studied the strategy adopted for forensic structural engineering after a bridge failure. Yilmaz et al. [3] investigated the effects of the changes in the coefficient of variation of probabilistic scouring variables and probability distributions on the probability of the loss of stability around dual bridge piers. Kovačević et al. [4] compared and analysed seven state-of-the-art machine learning techniques for estimating the construction costs of RC bridges. Wang [5] thoroughly described the monitoring system used at the Junshan Yangtze River Bridge. Here, the focus was mainly on the selection of monitoring variables, arrangement of sensor points, data collection and transmission system, data storage and management strategy and user interface system.

Most of the bridges in Algeria were constructed before 2008 (the year of publication of the first version of the Algerian seismic regulation code for bridge structures RPOA 2008 [6]) and before the introduction of seismic standards. A significant number of these bridges need to be upgraded or reinforced owing to fatigue effects. National authorities have raised concerns regarding the maintenance of these bridges on critical roads after a significant earthquake.

However, owing to the uncertainties of the ground motions and dynamic characteristics of bridges, probabilistic methods are widely used to assess the seismic performance of bridge structures. A seismic risk assessment addresses the structural vulnerability, hazard of the event and loss caused by the event in terms of lives and economic impact. A fragility curve is a type of seismic vulnerability tool used in risk assessment.

In this regard, the Pacific Earthquake Engineering Research Centre (PEER) developed a framework for a primary probability method for seismic design and assessment based on performance. The fundamental framework of the seismic fragility analysis of structures is based on the reliability theory and its theoretical framework. It quantifies the structural seismic performance in a probabilistic manner and correlates the ground motion intensity

with the structural damage state from a macro perspective. Meanwhile, the intensity level of the ground motion depends on the ground-motion parameter adopted and the structure response uncertainty can be characterised through the intensity measure (IM). Therefore, it is essential to select an appropriate IM of ground motion parameters for bridge structure analysis with regard to seismic fragility.

The selection of the IM determines the degree of dispersion of the probabilistic model. Certain ground motion IMs related to peak values, durations, spectral characteristics and energy are available. In general, the existing IMs are divided into two typical classes: scalar and vector. Scalar IM refers to a single IM. A vector IM commonly involves at least two IM components for the existing vulnerability curves for RC bridges, mainly elaborated upon in scalar IM.

The reliability of the results obtained by a probabilistic approach depends on the uncertainty level of the probabilistic seismic demand models (PSDMs). This illustrates the relationship between ground motion IMs and engineering demand parameters (EDPs) and, in turn, depends on the IM selected. In this regard, many researchers have recommended certain metrics to evaluate the optimal IM. Efficiency, practicality, proficiency and sufficiency [7] were identified as the most common of these. Several IMs were suggested by numerous researchers for use in bridge engineering. Two of these that are used extensively are the PGA maximum ground acceleration and $Sa(T_1)$ spectral acceleration at the fundamental period of the structure.

PGA and $Sa(T_1)$ are referred to as the optimal IMs in the case of simple steel girder multi-span bridge class [8]. $Sa(T_1)$ was selected as the optimal IM for a high-speed rail bridge seismic fragility assessment [9, 10]. The peak ground velocity (PGV) is recommended as the optimal IM for a cable-stayed bridge subjected to both far and near-fault ground motions [11]. The PGV tends to be the optimal IM for conditioning PSDMs for isolated bridges subjected to pulse-like ground motions [12]. Three IMs (the peak ground acceleration (PGA), PGV and PGD) were studied to assess the fragility of a tall pier bridge system subjected to near-fault ground motions by considering a bridge prototype in China and selecting the PGV as the optimal IM owing to the efficiency, relative sufficiency and practicality [13]. The PGA, PGV and velocity spectrum intensity (VSI) of the horizontal component of the ground motion and acceleration spectrum intensities (ASIs) of both horizontal and vertical components were identified as the optimal IMs for multi-span continuous concrete box-girder bridges, which accentuate near-field earthquakes. The spectral acceleration at 1.0 s ($Sa_{1.0}$) was adopted as the optimal IM for a typical Algerian post-tensioned highway bridge [14]. Several researchers have proposed a novel IM. Bayat et al. [15] selected the average spectral acceleration (ASA) as the optimal IM for skewed highway bridges. It represents the average value of the S_a between a lower and upper structural period. It is suitable for use in an appropriate period range and the spectral acceleration at 0.3 sec ($S_a(0.3T_s, 5\%)$) for isolated bridges [16].

In terms of vector IMs, the use of two-parameter IMs for RC frame structures [17] and unreinforced masonry buildings [18] have been recommended.

For RC bridges, in the study of Li et al. [19], seismic fragility surfaces were applied to derive fragility functions for each bridge component and spectral acceleration at the first two periods of vibration modes. $Sa(T_1)$, $Sa(T_2)$ were selected as a vector-valued IM. Baker and Cornell [20] proposed the spectral acceleration in the fundamental period of vibration $Sa(T_1)$ and the measurement of the spectral shape, $R_{T_1, T_2} = Sa(T_2) / Sa(T_1)$. The spectral acceleration Sa and the difference ε between the spectral acceleration of a record and the mean of the ground motion prediction equation in the given period were considered as a vector IM [21].

However, vector-valued IM vulnerability functions for Algerian bridges are unavailable. Hence, it necessitates improvement and further development to achieve an integrated risk assessment for these bridges. In the context of these limitations, this study aimed to develop vector and scalar-valued vulnerability functions for performing a seismic vulnerability analysis and performance-based evaluation of an RC pier bridge considering the soil class specified in the Algerian bridge design code RPOA 2008 [6]. A set of incremental dynamic analyses was performed to capture the seismic response of the RC bridge piers through 60 ground motion records based on the shear wave velocity V_{s30} used for the soil classification in RPOA 2008 [6]. Then, 10 IMs were selected to determine the one that is optimal for use in the scalar vulnerability analysis. The fragility scalar curves were constructed in terms of the optimal IM, based on the correlation, efficiency, practicality, proficiency and sufficiency results for the selected IMs. Subsequently, the probability of exceedance of different damage states was obtained using vector-valued fragility functions. Finally, a comparative analysis was conducted with the results derived from scalar fragility functions. Thereby, an overview of the importance of the second IM in the seismic fragility analysis of a typical Algerian RC bridge pier is provided in this study.

2. Procedure for scalar- and vector-valued vulnerability analysis

In the present study, a set of incremental dynamic analyses (IDAs) [22] was carried out to generate scalar and vector fragility curves (which are based on numerical analysis) for RC bridge piers. The schematic overview of the proposed procedure is shown in Figure 1 with the following eight steps:

1. Select a representative Algerian bridge design that features a geometry and pier shape.

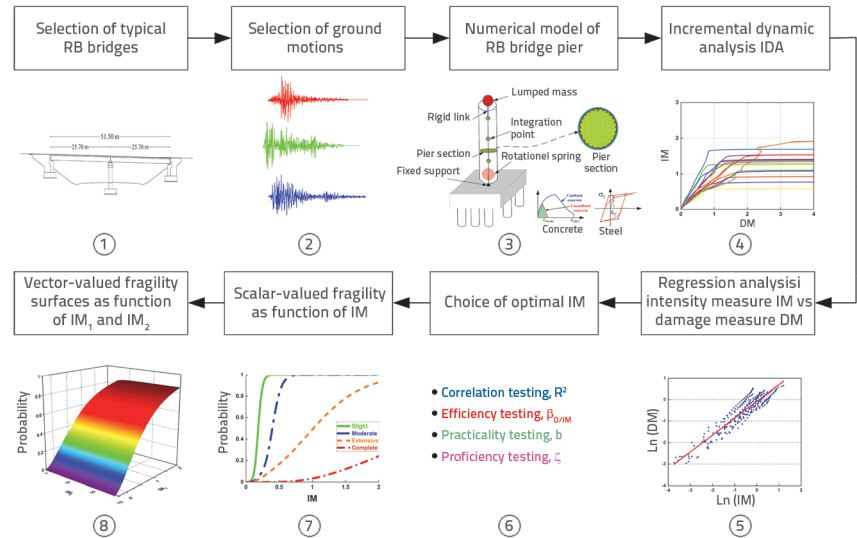


Figure 1. Overview of procedure for developing scalar- and vector-valued fragility functions of RC bridge piers

2. Select a suite of ground motions with sufficient accuracy to determine the seismic demand of the selected bridge.
3. Construct a numerical model of RC bridge piers according to the geometry and shape of the selected piers.
4. Perform a set of IDAs using numeric model step (3) and estimate the damage measure (DM) with the selected IM for the bridge piers investigated.
5. Set up the regression models between the selected IM and DM.
6. Identify the most appropriate IM required for the scalar fragility analysis while conducting the correlation, efficiency, practicality and proficiency tests
7. Develop a scalar-valued fragility function using the optimal IM obtained in step (6) for the investigated bridge.
8. Develop the vector-valued fragility function for the considered bridge based on two IMs.

3. Definition of scalar and vector fragility functions

Bridge seismic fragility refers to the conditional probability that the element response attains or surpasses certain specified damage limit state induced by multiple earthquakes at varying intensity levels.

A theoretical analysis method employing the reliability probability principle was considered in this study to investigate the seismic fragility of RC bridge piers.

Here, S_d is the seismic demand and S_c is the structural capacity. The probability of the seismic fragility of the RC piers can be expressed as shown in Eq. (1) [23]:

$$P_f = P \left[\frac{S_d}{S_c} \geq 1 \right] = P \left[\ln \frac{S_d}{S_c} \geq 0 \right] \quad (1)$$

Table 1. Threshold values of different damage measures

Damage measures	Threshold values				References
	Minor	Moderate	Extensive	Collapse	
Curvature ductility	1	1.18	3.22	4.18	[25]
	1	2.73	4.54	6.5	[26]
Displacement ductility	1	1.2	1.76	4.76	[27]
Drift [%]	2.25	2.9	4.6	5	[28]
	0.46	0.72	1.05	4.91	[29]
	1	1.22	1.78	4.8	[30]
	0.7	1.5	2.5	5	[31]

3.1. Scalar-valued fragility function

In previous studies, S_d and S_c have been assumed to follow a lognormal distribution. Therefore, $\ln(S_d / S_c)$ follows the normal distribution. Whether a linear regression analysis between $\ln(IM)$ and $\ln(S_d / S_c)$ is carried out, the mean λ (Eq. (2)) and standard deviation σ can be expressed as shown in Eq. (3):

$$\lambda = a \ln(IM) + b \tag{2}$$

$$\sigma = \sqrt{S_r / (n - 2)} \tag{3}$$

$$S_r = \sum_{i=1}^N [\ln \lambda_i - \ln(aIM_i^b)]^2 \tag{4}$$

where a and b are the linear regression coefficients and S_r is the sum of squares of the residuals for the regression plane for scattered points (Eq. (4)).

Eq. (1) can be transformed into a standard normal distribution form [24]:

$$P_f = P\left[\frac{S_d}{S_c} \geq 1\right] = 1 - \phi\left(\frac{\ln(IM) - \lambda}{\sigma}\right) = \phi\left(\frac{\lambda}{\sigma}\right) \tag{5}$$

ϕ is the standard normal cumulative density function. λ and σ are two parameters of the random DM distribution.

3.2. Vector-valued fragility function

In the case where the IM uses two parameters in the vector form $IM = (IM_1, IM_2)$, the mean and standard deviation of $\ln(S_d / S_c)$ can be expressed by Eq. (6). Here, a , b and c are linear regression coefficients.

$$\lambda = a \ln(IM_1) + b \ln(IM_2) + c \tag{6}$$

$$\sigma = \sqrt{S_r / (n - 3)} \tag{7}$$

By substituting Eq. (6) and Eq. (7) in Eq. (5), the fragility function of a bridge component with vector values is defined by

$$p_f = \phi\left(\frac{a \ln(IM_1) + b \ln(IM_2) + c}{\sqrt{S_r / (n - 3)}}\right) \tag{8}$$

4. Damage states and measures

The DM is assumed to quantify the seismic damage state (DS) of any structural element, such as bridge piers, exposed to seismic hazards. Hence, various quantitative definitions of the limit states of bridge damage are available in several codes. In the case of bridge piers, the curvature ductility [25, 26], displacement ductility [27] and drift [28-30] are commonly employed. Presently, no quantitative damage limit state measurements are available for Algerian bridges.

The different damage measures and threshold values used in the assessment of the fragility of bridge piers by several researchers are summarized in Table 1. In this study, a drift was selected as a DM. Furthermore, the limit states [31] were selected to define the bridge pier drift limits. Four qualitative damage limit states were defined: minor, moderate, extensive and collapse. Wherein it correlated with the drift limits values considered for the bridge piers was 0.7 %, 1.5 %, 2.5 % and 5 %.

5. Numerical modelling

5.1. Selected bridge

An existing post-tensioned highway bridge girder with two-span simply supported structure and a total length of 51.50 m was selected for the scalar- and vector-valued fragility analysis of reinforced concrete bridge piers. Each span was 25.70 m long and was isolated by elastomeric rubber bearings placed below the concrete girder supported on top of the RC pier cap. The superstructure consisted of a 200 mm thick and 10 m wide RC deck slab with an 80 mm wearing surface of asphalt layer. It was supported by seven

I-type girders placed on 0.05 m-thick elastomeric bearings measuring 0.30 x 0.30 m in the plan. The bridge pier bents were formed of three circular columns, each of diameter 1.40 m and height 7.00 m and a cap beam with a length of 12.00 m and a section of 2.00 x 1.00 m. Two shear keys were located at the abutment level. There was a 10 cm longitudinal gap between the deck and abutments and a 6 cm gap between shear keys and girders. The pier reinforcement consisted of twenty-seven longitudinal reinforcement bars of 32 mm diameter and reinforcement spirals of diameter 20 mm at 15 mm spacing. Rigid spread footings supported the bents and abutments. In addition, two rigid backfilled abutments had been constructed to support the deck and retain the embankment. The bridge bent configuration and geometry are shown in Figure 2.

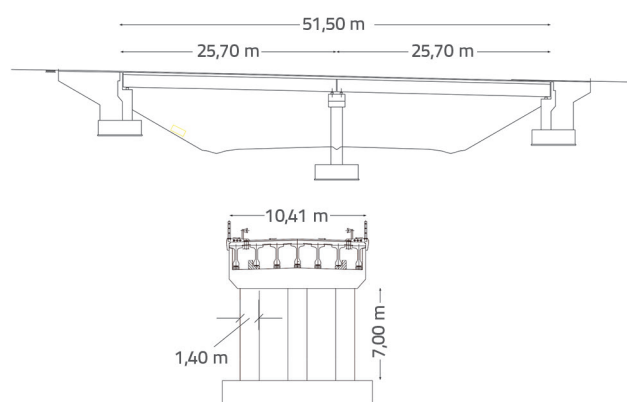


Figure 2. Configuration and geometry of the selected bridge

5.2. Numerical model

A numerical model capable of capturing nonlinearities in bridge components and materials is required to accurately quantify bridge seismic responses in global displacements. SeismoStruct software [32] was used to perform the seismic evaluation of the case study bridge. It allows for the visualisation of the damage pattern under various earthquake events. It is also used to predict the structural displacement behaviour of structures subjected to static and dynamic loading. The software has been used in previous research involving the seismic performance of RC bridges.

A three-dimensional (3D) model was developed for the bridge. It incorporates both material and geometric nonlinearities. In addition, in this study, the nonlinearity of the material was supposed to be based on the behaviour laws for concrete and steel reinforcement (derived as per the studies of Mander et al. [33] and Menegotto and Pinto [34], respectively). It is noted that the steel model was modified by Filippou et al. [35] to include the Bauschinger effect, which captures the stiffness degradation under cyclic loading.

The properties of concrete defined in SeismoStruct software [32] are a compressive strength (f_c) of 27 MPa, tensile strength (f_t) of 2.2 MPa, modulus of elasticity (E_c) of 24421.92 MPa, strain

at peak stress (ϵ_c) of 0.002 and specific weight (γ) of 24 kN/m³. Furthermore, the parameters introduced in the model of steel reinforcement are as follows: a yield strength (f_y) of 420 MPa, an elastic Young's modulus (E_s) of 200000 MPa and a strain-hardening ratio (R) of 0.005.

The bridge piers were embedded with plasticity elements distributed according to FB formulations based on inelastic force across fibre sections. The pier section discretisation resulted in a 250-fibre with five Gauss-Lobatto quadrature integration points.

The cap beam was modelled as an elastic linear beam element connected to the piers by rigid links in both longitudinal and transverse directions. A linear elastic beam element with mass distributed along the axis of the superstructure was employed for the deck. It was computed across an equivalent cross-section for the deck (slab and girders). A rigid link was applied to connect the slab and girders.

To define the elastomeric bearing model, a spring element was employed in both longitudinal and transverse directions and connected to a girder through rigid links. Effective stiffness K_{bear} and rotational stiffness K_q of 2160 kN/m and 5000 kN/rad, respectively, were used in the SeismoStruct software [32].

To describe the active and passive action of the abutment, three translational and three rotational linear spring elements were employed to depict both spring and dashpot elements connected to the deck. A proposed abutment model developed by Aviram et al. [36] was used in the analysis. In this model, a rigid elastic frame element and set of translational springs were used in the longitudinal, transverse and vertical directions in place of the abutment. In addition, the length of the rigid elastic frame element was equal to the width of the superstructure. Link elements that include three translational springs were connected at the ends of the rigid frame element.

The abutment is assumed to be designed as perfectly elastic. The stiffness of the abutment is given by Eq. (9) [37]:

$$K_{abut} = K_w(h_{bw}/1,7) \quad (9)$$

where K_{abut} is the initial abutment stiffness adjusted to the backwall height, K_i is the initial abutment stiffness based on test results (11.5 kN/mm/m) (Caltrans Seismic Design Criteria recommends a value of 14.35 kN for K_i [38]), w is the backwall width and h_{bw} is the backwall height. A linear gap/hook element defined in SeismoStruct [32] was used to model the gap between the deck and abutment.

The shear keys were designed to remain elastic under seismic excitations. The assumption was that the shear keys contribute to the stiffness in the transverse direction after the transverse displacement occurs at the gap value. This prevents excessive transverse displacement of the deck. Shear keys and a gap between shear keys and girder existed at abutment level 2. A spring element was used and shear keys stiffness at the pier K_{skew} was chosen as 500000 kN/m and for the abutments is equal to the half of stiffness pier shear keys.

Two lines with seven bearings each were present at the pier top level. Thus, the total stiffness was considered to be fourteen times the stiffness of an individual bearing. In addition, there are two shear keys in each line, i.e., the total is four. The two lines of bearings were simplified to one. Figure 3 shows an analytical model of the typical bridge.

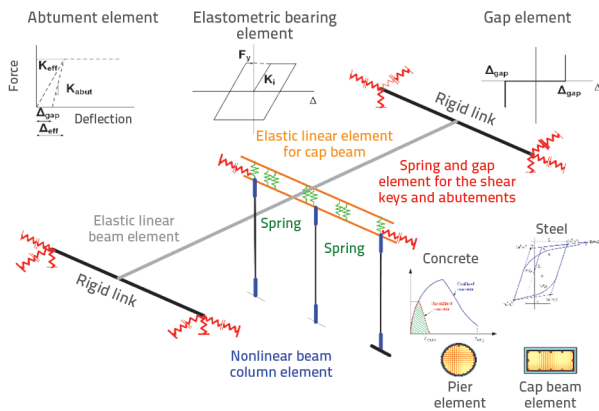


Figure 3. Numerical model of bridge

5.3. Selection of ground motions

It is essential to select appropriate ground motions to develop fragility surface curves for RC bridge piers. In this study, the design and calculation for bridge structures were performed according to the Algerian seismic regulation code for bridge structures RPOA 2008 [6].

In Algeria, the seismic zones are classified as I, IIa, IIb and III. Furthermore, four soil types are defined: S1 (hard rock), S2 (dense), S3 (soft) and S4 (very soft). These classifications are based on the shear velocity V_{s30} . Sixty ground motions were selected from the NGA-West2 earthquake database [39] and classified into four sets (see Figure 4).

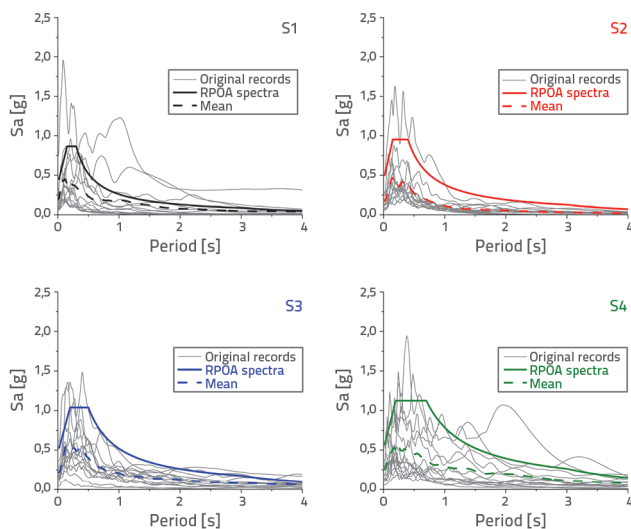


Figure 4. Classification of ground motions according to RPOA 2008 spectrum

Each set contains 15 ground-motion records. These ground motions were selected based on

- The shear wave velocity of the 30 m soil layer (V_{s30}): $V_{s30} > 800$ m/s for S1, 400 m/s $< V_{s30} < 800$ m/s for S2, 200 m/s $< V_{s30} < 400$ m/s for S3 and 100 m/s $< V_{s30} < 200$ m/s for S4.
- Magnitude (M_w): $5 < M_w < 8$,
- Hypocentral distance (R): $5 < R < 100$ km.

The details of the selected ground motion sets in terms of the magnitude M_w , distance R , PGA and shear velocity V_s are illustrated in Figure 5.

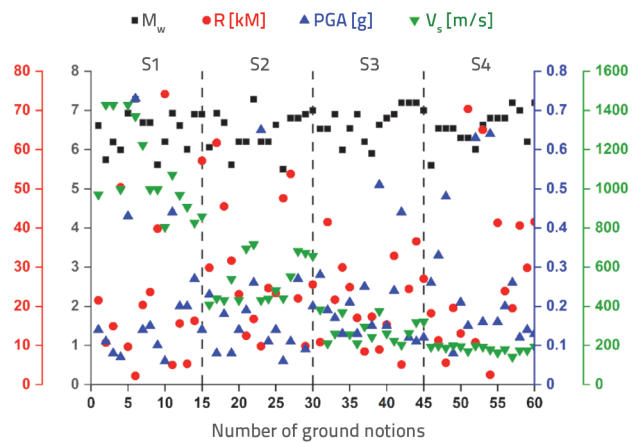


Figure 5. Classification of ground motions according to M_w , R , PGA and V_s

A significant step in the development of fragility curves is to match the selected motion records in terms of the spectral characteristics to ensure an accurate representation of the seismic hazard in the selected records. Furthermore, this spectral matching provides a highly effective tool to ensure that the scaling factors remain consistent during the IDA. SeismoMatch software [40] was used to conduct this process. Each accelerogram was adjusted according to the specific target response spectrum in this matching procedure without significant variation in frequency.

Matching was conducted in the period range, which was assumed to be from T_1 to T_2 as specified in RPOA 2008 [6]. Here, T_1 is the lower limit and T_2 is the upper limit of the constant spectral acceleration period. The different response spectra related to the period of the soil are tabulated in Table 2. No requirements are specified in Sections 4.3.3.2 and 4.3.3.3 (time history analysis and non-linear time-history analysis) of RPOA 2008 [6] for the scenario wherein the fundamental period exceeds the T_2 value of the seismic response spectrum.

Table 2. Values of T_1 and T_2 in RPOA 2008

Period	Site class			
	S1	S2	S3	S4
T_1 [s]	0.15	0.15	0.20	0.20
T_2 [s]	0.3	0.4	0.5	0.7

According to the RPOA 2008 [6], the normalised acceleration spectrum is given by Eq. (10):

$$S_{ae}(T, \xi)_{(m/s^2)} = \begin{cases} AgS[1 + (T / T_1)(2.5\eta - 1)] & 0 \leq T \leq T_1 \\ 2.5\eta AgS & T_1 \leq T \leq T_2 \\ 2.5\eta AgS(T_2 / T) & T_2 \leq T \leq 3.0 \\ 2.5\eta AgS(3T_2 / T^2) & 3.0 \leq T \end{cases} \quad (10)$$

where:

- $S_{ae}(T)$ - the elastic spectral acceleration
- T - the vibration period
- g - the gravitational acceleration (= 9,81 m/s²)
- A - the acceleration coefficient of the zone
- S - the soil factor
- η - a correction factor for the damping ratio ζ .

The mean response spectrum of the matched ground motion records and the target response spectrum are shown in Figure 6.

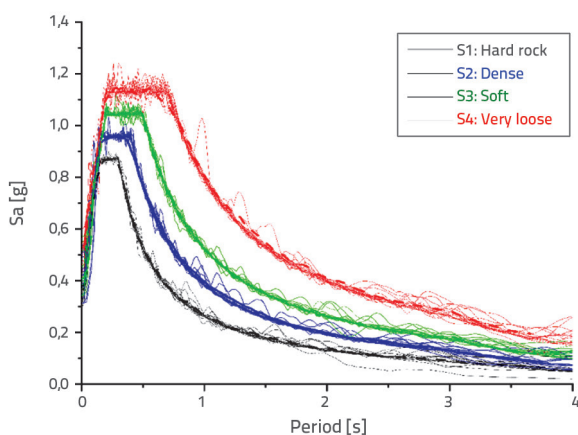


Figure 6. Mean response spectra matched with the RPOA 2008 spectrum

5.4. Modal analysis

A modal analysis was conducted on the model bridge to understand its dynamic characteristics. Modal response results including modal periods served as the main parameters in the response spectrum analysis and time history analysis.

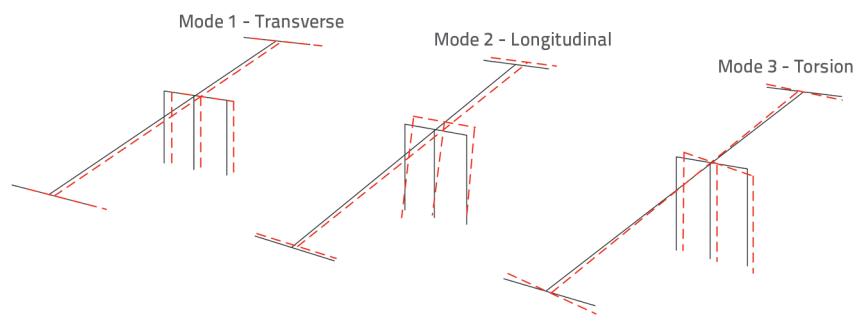


Figure 7. Mode shapes of selected bridge

Therefore, the seismic demand and structural response of the bridge could be evaluated efficiently.

Figure 7 illustrates that the principal mode shapes of the study involve the transverse and longitudinal translation and global torsion of the bridge. Table 3 summarises the modal analysis results including the periods and frequencies. Table 3 displays the period values for modal analysis.

Table 3. Modal analysis results

Mode	Mode 1	Mode 2	Mode 3
Period [s]	1.182	0.743	0.587
Frequency [Hz]	0.846	1.346	1.703

6. Fragility analysis

6.1. Scalar-valued fragility functions

6.1.1. Selection of examined seismic intensity measures

Various potential IMs were examined and the optimal one for analysis was selected to predict the response of RC bridge piers. Subsequently, the impact of the optimal IM on the fragility curve development was investigated.

This study used a collection of ten widely used IMs including amplitude and spectrum parameters, to investigate and select the most suitable IMs (Table 4). IMs are generally classified into acceleration, velocity and displacement types based on the physical properties. PGA, ASI, Sa(T₁), Sa_{0.2}, Sa_{1.0} and I_a are categorized as acceleration type; PGV, VSI and CAV are categorized as velocity type and PGD is categorized as displacement type.

6.1.2. Correlation analysis

The correlation of the IMs considered was analysed by a linear regression between ln (DM) and ln (IM). R² represents the correlation coefficient. It is an indicator of the accuracy of the regression in Eq. (2) and matches the computed seismic demand of the RC bridge piers. Figure 8 illustrates the regression analysis between the ten selected seismic IMs and the DM.

Following the above introduction, an optimal IM was assumed to have higher R² values than the other IMs. For the 10 IMs considered in Table 4, the calculated R² values for the DM are displayed in Figure 9. Sa(T₁, 5 %) is the most correlated IM among those examined. It is followed by VSI and ASI. The corresponding R² values are 0.974, 0.954 and 0.944, respectively. It can be demonstrated that the R² values are close to unity. Furthermore, the lowest correlation of IM with DM (see Figure 9) is for PGD, with R² = 0.543. It is followed by I_a and CAV (R² = 0.8 and 0.81, respectively).

Table 4. Intensity measures used in the analysis

No	Symbol	Eq.	unity	Description
1	PGA	$\max(\ddot{u}(t))$	g	Peak ground acceleration [41]
2	PGV	$\max(\dot{u}(t))$	m/s	Peak ground velocity [41]
3	PGD	$\max(u(t))$	m	Peak ground displacement [41]
4	CAV	$\int_0^{t_0} (\ddot{u}(t)) dt$	m/s	Cumulative absolute velocity [41]
5	I_a	$\frac{\cos^{-1} \xi}{g\sqrt{1-\xi^2}} \int_0^{t_0} (\ddot{u}(t)) dt$	m/s	Arias intensity [42]
6	$Sa(T_1, 5\%)$	$S_o(T_1, \xi)$	g	Spectral acceleration in the first period
7	$Sa_{0.2}$	$S_o(T_{0.2}, \xi)$	g	Spectral acceleration at 0.2 s
8	$Sa_{1.0}$	$S_o(T_{1.0}, \xi)$	g	Spectral acceleration at 1.0 s
9	ASI	$VSI = \int_{0.1}^{0.5} S_o(T, \xi = 5\%) dT$	$g*s$	Acceleration spectrum intensity [43]
10	VSI	$VSI = \int_{0.1}^{2.5} S_v(T, \xi = 5\%) dT$	m	Velocity spectrum intensity [43]

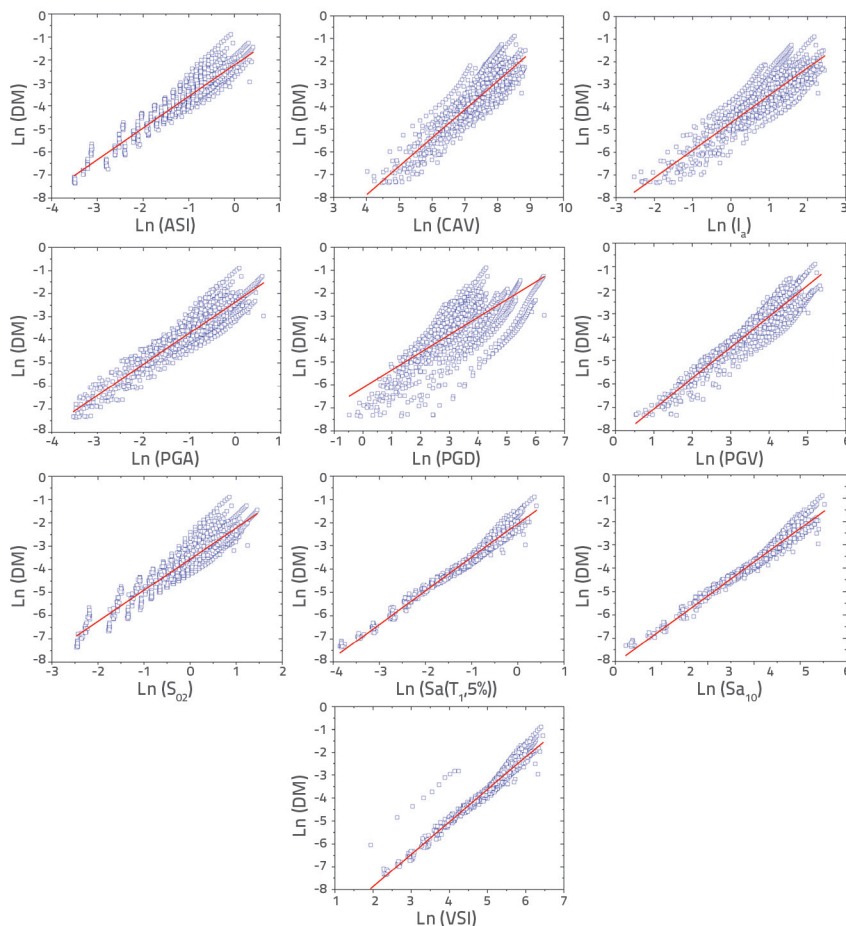


Figure 8. Regression analysis for the 10 IMs

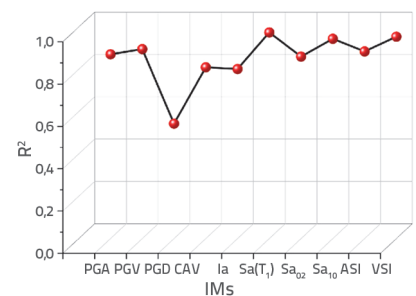


Figure 9. Regression parameter R² for the 10 IMs

6.1.3. Efficiency analysis

An efficient IM for a given DM for a specific purpose has the potential to decrease the variation in the seismic demand estimate. A lower standard deviation $\beta_{D/IM}$ (see Eq. (11)) indicates a more efficient IM:

$$\beta_{D/IM} = \sqrt{\frac{\sum_{i=1}^N [\ln(DM_i) - \ln(aIM_i^b)]^2}{N-2}} \quad (11)$$

The calculated standard deviations $\beta_{D/IM}$ for the 10 IMs are illustrated in Figure 10. From the above, it is concluded that $Sa(T_1, 5\%)$ is the most efficient IM with the lowest standard deviation (0.198). In addition, VSI and $Sa_{1.0}$ are the most

efficient IM among those evaluated. For the other IMs, the $\beta_{D/IM}$ values are 0.206 and 0.399, respectively. Meanwhile, the PGD has the lowest efficiency, with the highest standard deviation (0.832) among the IMs investigated. It is followed by I_a and CAV (0.547 and 0.538, respectively).

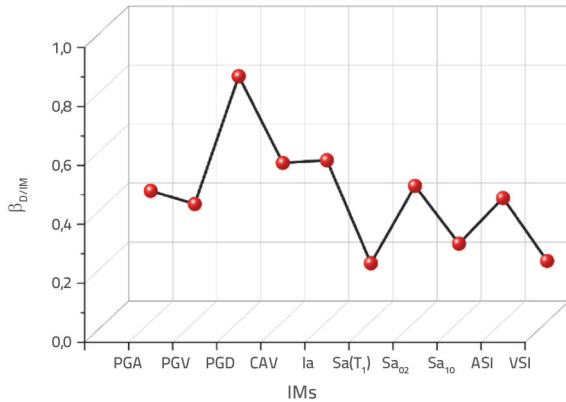


Figure 10. Regression parameter $\beta_{D/IM}$ for the 10 IMs

6.1.4 Practicality analysis

A measure of the dependence of the structural response demand on IM is practicality. The slope b in Eq. (2) is used to depict this dependence. It generally fits only the linear regression model. A higher b indicates that the IM examined contributes more significantly to the structural response demand. Therefore, this IM is more practical. The calculated slopes b for the IMs examined are shown in Figure 11. The figure shows that $Sa(T_1, 5\%)$, the VSI and Sa_{10} are the most practical IMs. Their b values are 1.445, 1.442 and 1.346, respectively. Meanwhile, the PGD, I_a and the CAV are the least practical of the IMs reviewed, with b values of 0.769, 1.211 and 1.255, respectively.

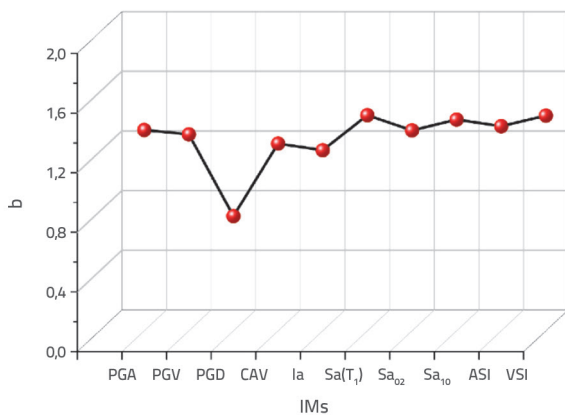


Figure 11. Regression parameter b for the 10 IMs

6.1.5. Proficiency analysis

According to Eq. (12), the proficiency ζ represents a compound measurement of the practicality and efficiency. A lower value of ζ is typically provided with a more efficient IM.

$$\zeta = \frac{\beta_{D/IM}}{b} \tag{12}$$

The resulting calculation of the 10 IMs examined is shown in Figure 12. From this, $Sa(T_1, 5\%)$ is the most proficient IM, as demonstrated by the lowest value of 0.137. It is followed by VSI and Sa_{10} with values of 0.143 and 0.303, respectively. However, the PGD is the least proficient measure (1.082) among the IMs examined. It is followed by I_a and CAV (0.452 and 0.428, respectively).

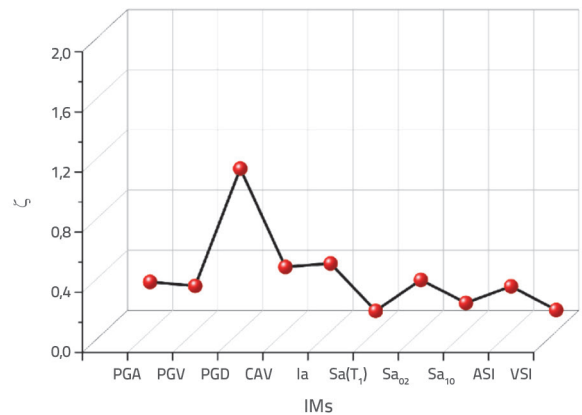


Figure 12. Regression parameter ζ for the 10 IMs

6.1.6. Selection of optimal intensity measures

Table 5 reveals the three IMs to be the most correlated, efficient, practical and proficient based on the previous analyses. $Sa(T_1, 5\%)$, the VSI and Sa_{10} appeared to be the best seismic IMs for the vulnerability analysis of the selected RC bridge piers. In this study, the optimal IM was $Sa(T_1, 5\%)$. It had the highest correlation, efficiency, practicality and proficiency.

Table 5. The regression parameters

IM	A	b	R ²
PGA	2.382	1.346	0.871
PGV	8.391	1.317	0.9
PGD	6.120	0.769	0.543
CAV	12.908	1.255	0.809
I_a	4.702	1.211	0.801
$Sa(T_1, 5\%)$	2.046	1.445	0.974
Sa_{02}	3.583	1.343	0.86
Sa_{10}	2.304	1.416	0.884
ASI	2.225	1.371	0.944
VSI	10.702	1.442	0.954

6.1.7. Proposed scalar-valued fragility functions

According to Table 4, a seismic fragility analysis and an earthquake damage assessment of the typical RC bridge piers

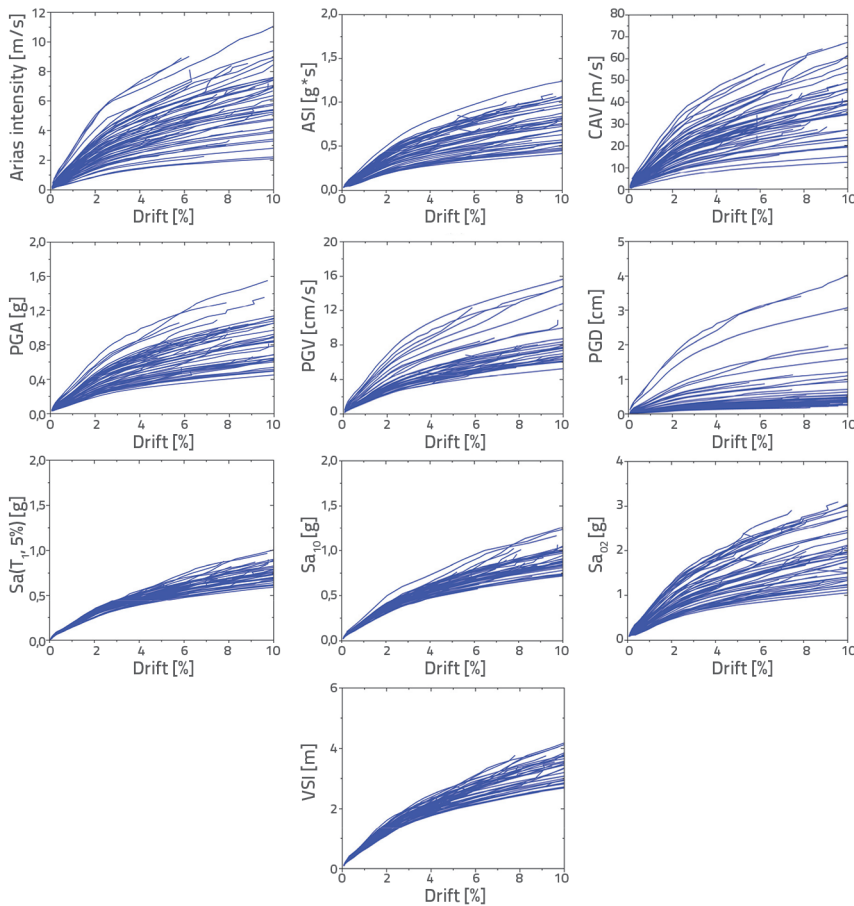


Figure 13. IDA curve of the selected RC pier bridges for the 10 IMs

the IDA curves. The step size of the selected ground motion in this work was 2 g and the step size increment was 0.1 g. Figure 13 shows The IDA curve of the selected RC bridge piers according to the IDA of the calculation of the 10 examined IMs. It can be concluded from Figure 13 and Table 5 that $Sa(T_1, 5\%)$ is a scalar-valued fragility function. The mean and standard deviation of the fragility functions for the bridge pier in four limit/damage states are presented in Table 6.

Table 6. Mean and standard deviation of fragility

Damage	Mean (λ)	Standard deviation (σ)
Minor	0.58	0.198
Moderate	0.62	0.198
Extensive	1.02	0.195
Collapse	2.65	0.191

The fragility curves for minor, moderate, extensive and collapse damage in terms of scalar-valued IM $Sa(T_1, 5\%)$ are illustrated in Figure 14.

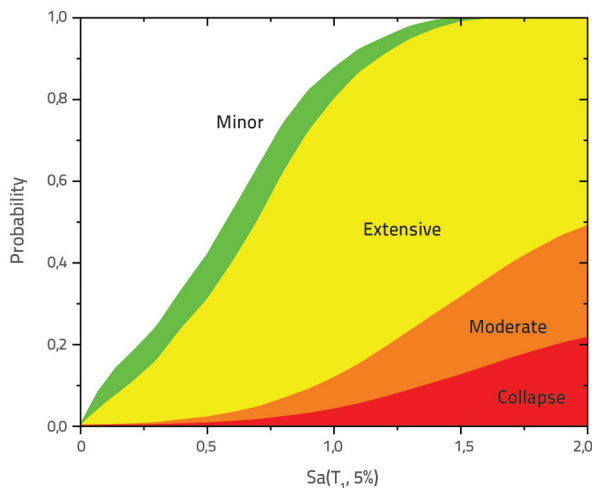


Figure 14. Scalar-valued fragility curves for RC pier bridges in terms of $Sa(T_1, 5\%)$

were performed by implementing IDA [22]. IDA is widely used to evaluate the performance of bridges and components subjected to earthquakes [29, 44, 45].

A series of ground motion data is fed into the model with increasing intensity until a structural deficit is identified. A relationship between the IM and the structural damage indicator DM can be observed in

6.2. Vector-valued fragility functions

Assume that an IM vector is composed of IM_1 and IM_2 and that $\ln(IM)$ follows a linear relationship with $\ln(EDP)$. Thus, this relationship can be represented as a multiple linear regression model:

$$\ln(EDP) = b_0 + b_1(IM_1) + b_2(IM_2) \tag{13}$$

The Pearson correlation coefficients between the different IMs were determined using Eq. (14). R^2 is a statistical measure that reflects the predictive power of the regression equation and measures its success:

$$R^2 = 1 - \frac{\sum [\ln(EDP_i) - \ln(\hat{EDP})]^2}{\sum [\ln(EDP_i) - \ln(\hat{EDP})]^2} \tag{14}$$

where $\ln(\hat{EDP})$ is the logarithmic regression mean of the EDP; $\ln(EDP_i)$ is the logarithmic value of the sample of EDP; and b_0 , b_1 and b_2 represent the regression coefficients.

The correlations obtained using multiple linear regression analysis are illustrated in Figure 15. The figure shows various colours corresponding to the correlation coefficients. The

IMs whose values are close to one were selected as vectors. The pairs $Sa(T_1)$ - Sa_{10} , $Sa(T_1)$ -VSI and Sa_{10} -VSI indicate high correlations (1, 0.99 and 0.99, respectively). Meanwhile, the pairs $PGD-I_a$, $PGD-CAV$ and $PGD-Sa_{0.2}$ exhibit weak correlations (0.56, 0.59 and 0.66, respectively).

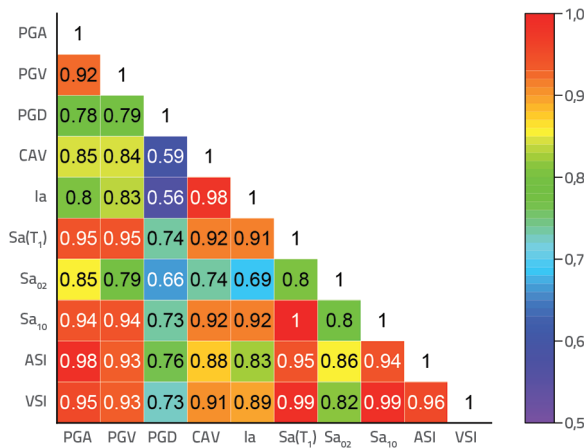


Figure 15. Pearson's coefficient of multiple correlations

The selection principle of the two IMs is to ensure that both are strongly correlated with the safety factor. In contrast, the correlation between the two measures should be minimum. These two conditions generally cannot be satisfied simultaneously [19].

For this study, based on the above and considering these two requirements synthetically, $Sa(T_1, 5\%)$ and VSI were designated as the spectrum IM and velocity IM, respectively. Therefore, $Sa(T_1, 5\%)$ and VSI were selected as vector-valued from the above selection principle of the two IMs. The damage measurement progression of the DM with both $Sa(T_1, 5\%)$ and VSI for the RC bridge piers studied is illustrated in Figure 16.

The scatter points depict the corresponding DM values under increasing intensity for the typical RC bridge piers investigated using the selected ground motions. The surface plot displays the regression fit surface for these DM values. It is shown in Eq. (15) with $R^2 = 0.991$ and standard deviation $\beta_{D|IM} = 0.154$:

$$\ln DM = 2,582 + 1,32 \ln Sa(T_1, 5\%) + 1,311 \ln VSI \quad (15)$$

The R^2 values in the case of the vector-valued IM ($Sa(T_1, 5\%), VSI$) are marginally higher than those in the case of a

scalar-valued IM (i.e. 0.974 for $Sa(T_1, 5\%)$ or 0.954 for VSI). This demonstrates that the vector-valued IM $Sa(T_1, 5\%), VSI$ has a better correlation relationship with the DM.

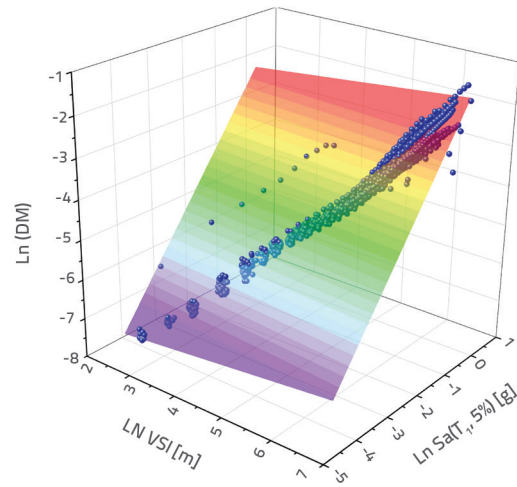


Figure 16. Evolution of the damage measure (DM) with $Sa(T_1, 5\%)$ and VSI

6.2.1. Proposed vector-valued fragility functions

There are various advantages of vector-valued IMs compared to scalar IMs for assessing the seismic demand by a probabilistic approach. One of these is that a vector-valued IM significantly reduces the fragility function dispersion. In contrast, considering only an intensity parameter and scalar-valued fragility curves can yield different exceedance probabilities, which depend on the selected IM. Coupling two IMs provides an opportunity to

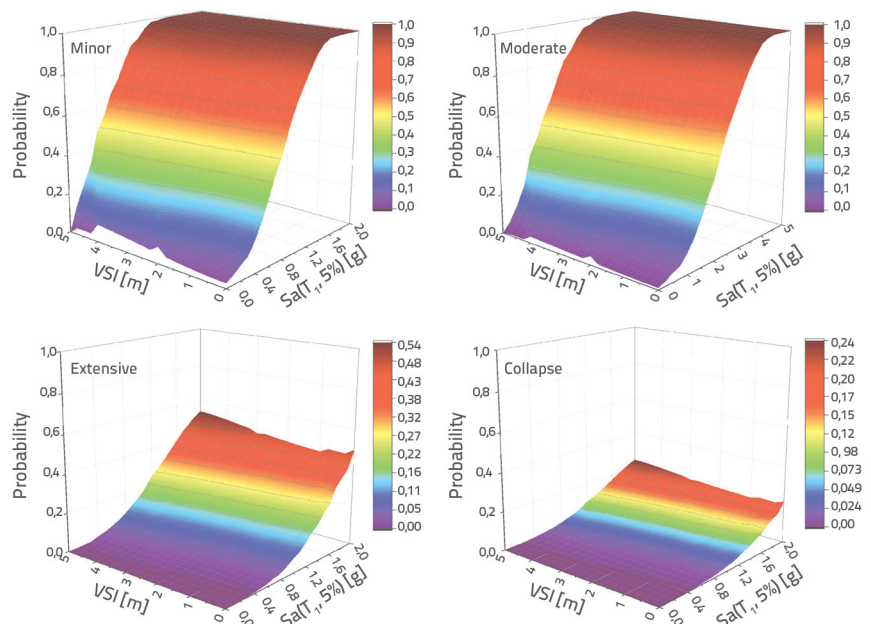


Figure 17. Vector-valued fragility surfaces for typical RC pier bridges based on $Sa(T_1, 5\%)$ and VSI

develop a robust fragility function in terms of standard fragility curves, which can be incorporated into seismic risk assessment. The minor, moderate, extensive and collapse damage fragility surfaces for the vector-valued IM ($Sa(T_1, 5\%)$, VSI) are depicted in Figure 17.

6.2.2. Comparisons of the scalar- and vector-valued fragility functions

The effect of the second IM was investigated based on fragility surfaces in this study. Univariate fragility curves were constructed with a constant second IM (VSI). In addition, the resultant and scalar fragility curves (constructed according to the first IM ($Sa(T_1, 5\%)$)) were compared.

The scalar and vector fragility surface intervals are compared in Figure 18 for minor, moderate, extensive and collapse damage. Here, the VSI constant is set to 1, 2, 3, 4 and 5 m, respectively. The vertical lines represent the values of $Sa(T_1)$ with the lower limit of the constant spectral acceleration period T_1 corresponding to the four soil classes S1, S2, S3 and S4 specified in the RPOA 2008 code [6].

A significant effect of the second IM for damage probability is observed numerically in the results. In addition, the fragility curves of scalar values can underestimate or overestimate the damage probability (as observed in Figure 18).

Fragility curves can induce an underestimated damage probability under earthquake events with $VSI > 3$ m. It generates an overestimated damage probability under seismic events with $VSI < 3$ m for the RC pier bridge.

This investigation of the RC bridge piers also demonstrated that vector-valued fragility curves have better and more relevant

information for evaluating the seismic performance, compared with scalar fragility curves.

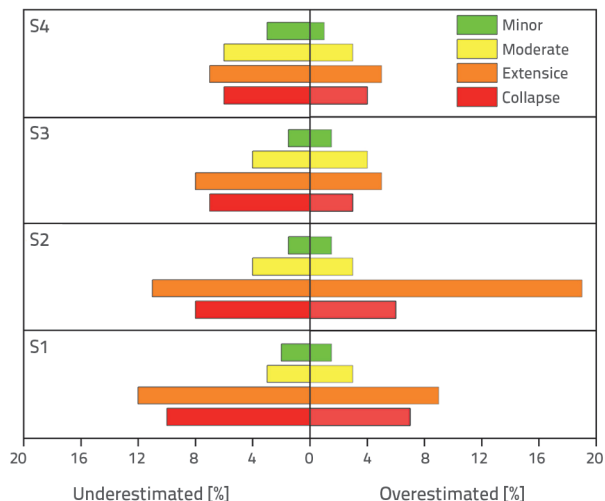


Figure 19. Underestimation and overestimation of the probability of the four damage states

Figure 19 summarises the underestimation and overestimation of the probability of the four damage states between the scalar and vector fragility surfaces for the four soil classes S1, S2, S3 and S4 specified in the RPOA 2008 code [6]. A high overestimated value of 19 % was observed in the extensive damage corresponding to the S2 soil and a high underestimated value of 12 % was observed in the extensive damage corresponding to the S1 soil.

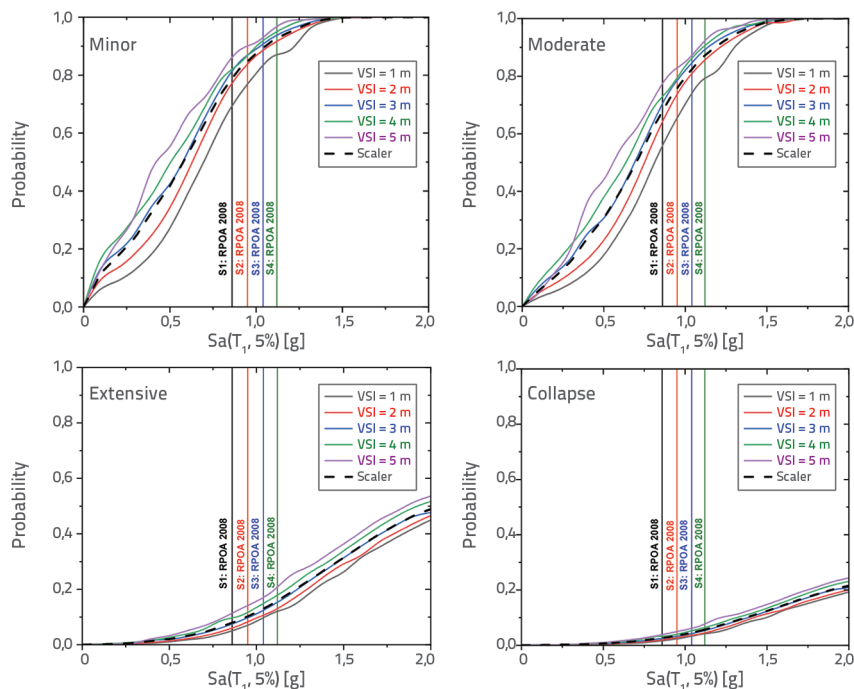


Figure 18. Comparison of fragility surface and fragility curve

7. Conclusion

The fragility of typical Algerian RC bridge piers was examined in this study. The seismic demands were calculated under 60 ground motions by numerical analysis. These were subsequently scaled to correspond to the RPOA 2008 spectrum.

A group of 10 IMs was selected and evaluated for multiple measures including correlation, efficiency, practicality and proficiency by performing a large number of regression analyses between the IMs and DM.

Using this approach, the optimal IM was recommended for analysing the seismic fragility of RC bridge piers. Next, vector-valued fragility functions were derived. This showed the relevance of the second IM in the bridge fragility analysis.

The following conclusions can be drawn from this study:

The correlation, efficiency, practicality and proficiency were examined based on the 10 selected IMs for a typical RC bridge pier. $Sa(T_1, 5\%)$, VSI and Sa_{10} were observed to be better IMs for fragility analysis with a scalar value. In addition, $Sa(T_1, 5\%)$ was identified as the optimal IM based on its high correlation, efficiency, practicality and proficiency compared to of the other IMs.

The fragility curves using scalar values for the optimal IM $Sa(T_1, 5\%)$ were developed. Vector-valued IMs based on the fragility functions were developed for the RC bridge piers to determine the exceedance probability of various damage states as a function of two IMs ($Sa(T_1, 5\%)$, VSI). Unlike a scalar IM, the vector IM composed of two IM $Sa(T_1, 5\%)$ and VSI displayed better correlation and efficiency toward the seismic demand.

The effect on the seismic performance owing to the second IM is not reflected fully by the scalar-valued fragility curve. Therefore, damage probabilities may be underestimated or overestimated. Although this study can be considered as universally applicable, the optimal seismic demand model computed herein is most applicable to the investigated bridge. Compared with a scalar IM, the vector IMs derived ensure a higher correlation between the IMs and DM and minimise the multicollinearity among the vector IMs.

Acknowledgements

This research was supported by the National Earthquake Engineering Research Center, CGS, Algeria.

REFERENCES

- [1] Zhou, X., Zhang, R., Zhao, K., Zhang, G., Wu, B.: An experimental study of impact performance of RC piers with different reinforcement ratios, *GRAĐEVINAR*, 71 (2019) 6, pp. 465-479, <https://doi.org/10.14256/JCE.2305.2018>
- [2] Milić, I., Ivanković, A. M., Syrkov, A., Skokandić, D.: Bridge failures, forensic structural engineering and recommendations for design of robust structures, *GRAĐEVINAR*, 73 (2021) 7, pp. 717-736, <https://doi.org/10.14256/JCE.3234.2021>
- [3] Yilmaz, M., Calamak, M., Yanmaz, A. M.: Reliability-based evaluation of scour around dual bridge piers, *GRAĐEVINAR*, 71 (2019) 9, pp. 739-747, <https://doi.org/10.14256/JCE.2363.2018>
- [4] Kovačević, M., Ivanišević, N., Petronijević, P., Despotović, V.: Construction cost estimation of reinforced and prestressed concrete bridges using machine learning, *GRAĐEVINAR*, 73 (2021) 1, pp. 1-13, <https://doi.org/10.14256/JCE.2738.2019>
- [5] Wang, C.: Overview of integrated health monitoring system installed on cable-stayed bridge and preliminary analysis of results, *GRAĐEVINAR*, 73 (2021) 6, pp. 591-604, <https://doi.org/10.14256/JCE.2940.2020>
- [6] RPOA: Règles Parasismiques Applicables au Domaine des Ouvrages d'Art. Document Technique Règlementaire. Ministère des Travaux Publics, Algiers. Alegria, 2008
- [7] Zelaschi, C., Monteiro, R., Pinho, R.: Critical Assessment of Intensity Measures for Seismic Response of Italian RC Bridge Portfolios, *Journal of Earthquake Engineering*, 23 (2019) 6, pp. 980-1000, <https://doi.org/10.1080/13632469.2017.1342293>
- [8] Padgett, J.E., Nielson, B.G., DesRoches, R.: Selection of optimal intensity measures in probabilistic seismic demand models of highway bridge portfolios, *Earthquake Engineering and Structural Dynamics*, 37 (2008) 5, pp. 711-725, <https://doi.org/10.1002/eqe.782>
- [9] Wei, B., Yang, T., Jiang, L., He, X.: Effects of uncertain characteristic periods of ground motions on seismic vulnerabilities of a continuous track-bridge system of high-speed railway, *Bulletin of Earthquake Engineering*, 16 (2018) 9, pp. 3739-3769, <https://doi.org/10.1007/s10518-018-0326-8>
- [10] Wei, B., Li, C., He, X.: The Applicability of Different Earthquake Intensity Measures to the Seismic Vulnerability of a High-Speed Railway Continuous Bridge, *International Journal of Civil Engineering*, 17 (2019) 7, pp. 981-997, <https://doi.org/10.1007/s40999-018-0347-3>
- [11] Zhong, J., Jeon, J.S., Shao, Y.H., Chen, L.: Optimal Intensity Measures in Probabilistic Seismic Demand Models of Cable-Stayed Bridges Subjected to Pulse-Like Ground Motions, *Journal of Bridge Engineering*, 24 (2019) 2, pp. 4018118, [https://doi.org/10.1061/\(ASCE\)BE.1943-5592.0001329](https://doi.org/10.1061/(ASCE)BE.1943-5592.0001329)
- [12] Jiang, L., Zhong, J., He, M., Yuan, W.: Optimal Seismic Intensity Measure Selection for Isolated Bridges under Pulse-Like Ground Motions, *Advances in Civil Engineering*, (2019) 3, pp. 1-22, <https://doi.org/10.1155/2019/3858457>
- [13] Chen, X.: System Fragility Assessment of Tall-Pier Bridges Subjected to Near-Fault Ground Motions, *Journal of Bridge Engineering*, 25 (2020) 3, pp. 4019143, [https://doi.org/10.1061/\(ASCE\)BE.1943-5592.0001526](https://doi.org/10.1061/(ASCE)BE.1943-5592.0001526)
- [14] Kehila, F., Remki, M., Zourgui, N.H., Kibboua, A.: Bechtoula H. Optimal intensity measure of post-tensioned girder highway bridge using fragility curves, *Earthquakes and Structures*, 20 (2021) 6, pp. 681-696, <https://doi.org/10.12989/eas.2021.20.6.681>
- [15] Bayat, M., Daneshjoo, F., Nistico, N.: A novel proficient and sufficient intensity measure for probabilistic analysis of skewed highway bridges, *Structural Engineering and Mechanics*, 55 (2015) 6, pp. 1177-1202, <https://doi.org/10.12989/SEM.2015.55.6.1177>
- [16] Bayat, M., Ahmadi, H.R., Kia, M., Cao, M.: Probabilistic seismic demand of isolated straight concrete girder highway bridges using fragility functions, *Advances in concrete construction*, 7 (2019) 3, pp. 183-189, <https://doi.org/10.12989/acc.2019.7.3.183>
- [17] Seyedi, D.M., Gehl, P., Douglas, J., Davenne, L., Mezher, N., Ghavamian, S.: Development of seismic fragility surfaces for reinforced concrete buildings by means of nonlinear time-history analysis, *Earthquake Engineering and Structural Dynamics*, 39 (2010), pp. 91-108, <https://doi.org/10.1002/eqe.939>
- [18] Gehl, P., Seyedi, D.M., Douglas, J.: Vector-valued fragility functions for seismic risk evaluation, *Bulletin of Earthquake Engineering*, 11 (2013) 2, pp. 365-384, <https://doi.org/10.1007/s10518-012-9402-7>
- [19] Li, Z., Li, Y., Li, N.: Vector-intensity measure based seismic vulnerability analysis of bridge structures, *Earthquake Engineering and Engineering Vibration*, 13 (2014) 4, pp. 695-705, <https://doi.org/10.1007/s11803-014-0273-6>

- [20] Baker, J.W., Cornell, C.A.: Vector-valued Intensity Measures Incorporating Spectral Shape for Prediction of Structural Response, *Journal of Earthquake Engineering*, 12 (2008) 4, pp. 534-554, <https://doi.org/10.1080/13632460701673076>
- [21] Tothong, P., Luco, N.: Probabilistic seismic demand analysis using advanced ground motion intensity measures, *Earthquake Engineering and Structural Dynamics*, 36 (2007) 13, pp. 1837-1860, <https://doi.org/10.1002/eqe.696>
- [22] Vamvatsikos, D., Cornell, C.A.: Incremental dynamic analysis, *Earthquake Engineering and Structural Dynamics*, 31 (2002) 3, pp. 491-514, <https://doi.org/10.1002/eqe.141>
- [23] Choi, E., DesRoches, R., Nielson, B.: Seismic fragility of typical bridges in moderate seismic zones, *Engineering Structures*, 26 (2004) 2, pp.187-199, <https://doi.org/10.1016/j.engstruct.2003.09.006>
- [24] Pan, Y., Agrawal, A.K., Ghosn, M., Alampalli, S.: Seismic Fragility of Multispan Simply Supported Steel Highway Bridges in New York State. II: Fragility Analysis, Fragility Curves, and Fragility Surfaces, *Journal of Bridge Engineering*, 15 (2010) 5, pp. 462-472, [https://doi.org/10.1061/\(ASCE\)BE.1943-5592.0000055](https://doi.org/10.1061/(ASCE)BE.1943-5592.0000055)
- [25] Ramanathan, K., DesRoches, R., Padgett, J.E.: A comparison of pre- and post-seismic design considerations in moderate seismic zones through the fragility assessment of multispan bridge classes, *Engineering Structures*, 45 (2012), pp. 559-573, <https://doi.org/10.1016/j.engstruct.2012.07.004>
- [26] Jara, J.M., Galván, A., Jara, M., Olmos, B.: Procedure for determining the seismic vulnerability of an irregular isolated bridge, *Structure and Infrastructure Engineering*, 9 (2013) 6, pp.516-528, <https://doi.org/10.1080/15732479.2011.576255>
- [27] Alam, S.M., Bhuiyan, R.M.A., Billah, A.H.M.: Seismic Fragility Assessment of SMA-Bar Restrained Multi-Span Continuous Highway Bridge Isolated by Different Laminated Rubber Bearings in Medium to Strong Seismic Risk Zones. *Bulletin of Earthquake Engineering*, 10 (2012), pp. 1885-1909, <https://doi.org/10.1007/s10518-012-9381-8>
- [28] Billah, A.H.M., Alam, M.S.: Seismic Fragility Assessment of Concrete Bridge Pier Reinforced with Super elastic Shape Memory Alloy. *Earthquake Spectra*, 31 (2015) 3, pp. 1515-1541, <https://doi.org/10.1193/112512EQS337M>
- [29] Kehila, F., Kibboua, A., Bechtoula, H., Remki, M.: Seismic performance assessment of R.C. bridge piers designed with the Algerian seismic bridges regulation, *Earthquakes and Structures*, 15 (2018) 6, pp. 701-713, <https://doi.org/10.12989/eas.2018.15.6.701>
- [30] Billah, A.H.M., Alam, S.M.: Seismic Fragility Assessment of Highway Bridges: a State-of-the- Art Review. *Structure and Infrastructure Engineering*, 11 (2014) 6, pp. 804-832, <https://doi.org/10.1080/15732479.2014.912243>
- [31] Dutta, A., Mander, J.B.: Seismic fragility analysis of highway bridges, *Proceedings of the center-to-center project workshop on earthquake engineering in transportation systems*, 1999.
- [32] SeismoStruct: A Computer Program for Static and Dynamic Nonlinear Analysis of Framed Structures. Available from <http://www.seissoft.com>. Last accessed August 2022.
- [33] Mander, J.B., Priestley, M.J.N., Park, R.: Theoretical Stress-Strain Model for Confined Concrete. *Journal of Structural Engineering ASCE*, 114 (1998) 8, pp 1804-1826, [https://doi.org/10.1061/\(ASCE\)0733-9445\(1988\)114:8\(1804\)](https://doi.org/10.1061/(ASCE)0733-9445(1988)114:8(1804))
- [34] Menegotto, M., Pinto, P.E.: Method of Analysis for Cyclically Loaded Reinforced Concrete Plane Frames Including Changes in Geometry and Non-elastic Behaviour of Elements Under Combined Normal Force and Bending, In: *IABSE Symposium on Resistance and Ultimate Deformability of Structures Acted on by Well Defined Repeated Loads*. Zurich, pp. 112-1231, 1973.
- [35] Filippou, F.C., Popov, E.P., Bertero, V.V.: Effects of Bond Deterioration on Hysteretic Behavior of Reinforced Concrete Joints, *Earthquake Engineering Research Center, University of California*, 1983.
- [36] Aviram, A., Mackie, K.R., Stojadinovic, B.: Effect of Abutment Modelling on the Seismic Response of Bridge Structures, *Earthquake Engineering and Engineering Vibration*, 7 (2008) 4, pp. 395-402, <https://doi.org/10.1007/s11803-008-1008-3>
- [37] Hemaidi Zourgui, N., Kibboua, A., Taki, M.: Using full bridge model to develop analytical fragility curves for typical concrete bridge piers, *GRADEVINAR*, 70 (2018) 6, pp. 519-530, <https://doi.org/10.14256/JCE.2137.2017>
- [38] Caltrans, SDC: *Caltrans Seismic Design Criteria version 1.4*. California Department of Transportation. Sacramento, California, 2006.
- [39] PEER - Pacific Earthquake Engineering Research Center.: *PEER NGA-West2 Database*. Report 2013/03. Berkeley. California, 2013.
- [40] SeismoMatch: A computer program for spectrum matching of earthquake records, Available from <http://www.seissoft.com>. Last accessed August 2022.
- [41] Kramer, S.L.: *Geotechnical earthquake engineering*. Upper Saddle River: Prentice Hall; 1996.
- [42] Arias, A.: A measure of earthquake intensity, in: *Seismic Design for Nuclear Power Plants*, edited by: Hansen, R. J., MIT Press, Cambridge, Massachusetts, 438-483, 1970.
- [43] Housner G.W. *Proceedings of the Symposium on Earthquakes and Blast Effects on Structures 1952*.
- [44] Tehrani P, Mitchell D. Seismic Response of Bridges Subjected to Different Earthquake Types Using IDA. *Journal of Earthquake Engineering*, 17 (2013) 3, pp.423-448, <https://doi.org/10.1080/13632469.2012.760500>
- [45] Mosleh, A., Jara, J., Razzaghi, M.S., Varum, H.: Probabilistic Seismic Performance Analysis of RC Bridges, *Journal of Earthquake Engineering*, 24 (2018) 11, pp.1704-1728, <https://doi.org/10.1080/13632469.2018.1477637>